Reaction Crystallization Kinetics of Benzoic Acid

Marie Ståhl, Bengt L. Åslund, and Åke C. Rasmuson
Dept. of Chemical Engineering and Technology, Royal Institute of Technology, SE-100 44 Stockholm, Sweden

Benzoic acid was crystallized in a T-mixer by mixing hydrochloric acid and an aqueous sodium benzoate solution. Crystallization kinetics were determined by population balance modeling and parameter estimation by nonlinear optimization. The evaluation of several models showed that the model has to be carefully designed. The objective function is highly nonconvex, and the results have to be scrutinized to identify the appropriate optimum. Growth-rate dispersion needs to be accounted for to obtain a reasonable description of experimental product-size distributions. Six parameters of nucleation and growth kinetics were determined simultaneously in an optimization that includes experimental product-size distributions from 14 experiments at 8 different initial supersaturations. The interfacial energy calculated from the corresponding nucleation parameter is 0.015 J/m^2. The exponent of the normal power law growth-rate equation receives a value of 2.1, suggesting that growth is controlled by surface integration. The value becomes 2.9 if the logarithm of the supersaturation ratio is used as the driving force. The coefficient of variation of the growth-rate distribution depends only weakly on supersaturation and receives a value of 0.23 if this dependence is neglected. The final model describes experimental data well. The estimated parameters are physically reasonable and provide a physically reasonable description of the entire experiment.

Introduction

Reaction crystallization (precipitation) is an important industrial process. Substances produced by precipitation include fine and bulk chemicals, especially pharmaceuticals, biochemicals, pigments, catalysts, and photographic materials. It is important to have knowledge of the proper crystallization kinetics when crystallization processes are designed and scaled up. However, in reaction crystallization, determination of kinetics is particularly troublesome because of the difficulties in separating the kinetics of crystallization from the influence of mixing. If the solution is not completely mixed before the crystallization starts, for example, if the reaction is fast, the crystallization proceeds under conditions of partial segregation. Local micromixing has a large influence on the generation of supersaturation, and local supersaturation ratios can reach values of several orders of magnitude. Under these conditions, nucleation and growth will be very rapid, and, thus, local micromixing will influence the crystallization as well. These interactions are complex, and nucleation and growth kinetics in reaction crystallization are poorly understood, as is the role of mixing.

Correspondence concerning this article should be addressed to A. C. Rasmuson.

Traditionally, reaction crystallization kinetics are studied by mixing reactant solutions in a beaker, and determining the induction time and/or the total number of product crystals produced (Nielsen, 1964, 1969; Mohanty et al., 1988; Bhandarkar et al., 1989; Söhnel and Mullin, 1988). Nielsen (1969) derived relationships relating this information to the rate of homogeneous primary nucleation for different crystal growth mechanisms.

To eliminate the influence of mixing on kinetics, reactants must be well mixed before the onset of nucleation. In an agitated beaker, the mixing time may be on the order of seconds, which, accordingly, restricts the level of supersaturation that can be studied. The mixing time can be reduced by letting the reactant streams impinge on each other as two opposed jets in a tee coupling. According to Söhnel and Garside (1992) the mixing time in a T-mixer with a two-stream mixing chamber can be about 2–3 ms at turbulent conditions. Several authors have studied induction times and total number of crystals produced in T-mixer experiments (Nielsen, 1961, 1967; Söhnel and Mullin, 1978; Mohanty et al., 1988; Bhandarkar et al., 1989; Mahajan and Kirwan, 1993; Schubert and Mersmann, 1996).

Kinetics can be evaluated by applying population balance modeling. Experimental data generally include product-size distributions and, in some cases, supersaturation profile information (Rivera and Randolph, 1978; Mahajan and Kirwan, 1993; Mignon et al., 1996). Rivera and Randolph (1978) mixed the reactants in a T-mixer and allowed the mixture to pass a static mixer, after which crystallization occurred. They used a model for dispersed plug flow to estimate effective kinetics. Mahajan and Kirwan (1993) used a grid mixer and measured the crystal size distribution at different residence times. A plug-flow model was used to extract kinetics. Mignon et al. (1996) used a T-mixer to mix reactants. The mixture was then led into a batch reactor where the precipitation continued. The experiment was modeled as a fed-batch reactor, and kinetics of growth and nucleation were extracted by optimization. Aoun et al. (1999) determined kinetic data from batch precipitation experiments. By nonlinear optimization, the nucleation rates were determined from measurements of the evolution of the crystal-size distribution, and the growth rate from the supersaturation profile. In the work by Nallet et al. (1998), a similar study was carried out on the batch precipitation of salicylic acid. The reactor was modeled as ideally mixed. Concentration measurements and final size distribution from three experiments were included in a parameter estimation by optimization.

The aim of the present work is to estimate the kinetics of the reaction crystallization of benzoic acid. Although most investigations on reaction crystallization kinetics have been carried out on inorganic systems, there is a considerable interest in the industry for kinetic data on organic systems as well. Benzoic acid is chosen as an organic model substance. Hydrochloric acid is mixed with an aqueous sodium benzoate solution in a T-mixer. A rigorous population-balance model of the crystallization that includes nucleation and crystal growth is developed, and kinetics are determined by nonlinear optimization. The optimization process is examined, and the model and kinetics are carefully evaluated. It is concluded that care must be exercised both in the design of the model, and in the determination of kinetics. It is also concluded that growth-rate dispersion can be an important feature of the growth kinetics in reaction crystallization. In all, four different models with increasing complexity have been assessed.

Theory

In the classic theory of primary nucleation, the number generation rate of homogeneous nucleation B_p is expressed as (Nielsen, 1964)

$$B_p = K_{p1} \exp\left(-\frac{\Delta G_{cr}}{kT}\right), \tag{1}$$

where ΔG_{cr} is determined as

$$\Delta G_{cr} = \frac{4k_a^3 \upsilon_m^2 \gamma_s^3}{27k_v^2 (kT \ln S)^2}. \tag{2}$$

Heterogeneous nucleation is usually described by the same formalism. However, the activation energy ΔG_{cr} is reduced by a constant in the equation, since the presence of particles is assumed to catalyze the nucleation. After supersaturation has been established, there is generally a time period before crystals can be detected in the solution. This time period is called the induction time, and it is assumed to be inversely proportional to the nucleation rate.

In order to determine the kinetics of homogeneous nucleation, Nielsen (1969) developed expressions describing the relationship between the nucleation rate and the induction time or the total number concentration. Since the crystals must grow to a detectable size, the particular growth mechanism has to be specified. When growth is controlled by diffusion, the obtained expression is

$$\log t_{\text{ind}} = K_{ti1} + \frac{2}{5} K_{ti2} (\log S)^{-2}, \tag{3}$$

where K_{ti2}, is given by

$$K_{ti2} = \frac{4k_a^3 \upsilon_m^2 \gamma_s^3}{27k_v^2 (\ln 10)^3 (kT)^3}. \tag{4}$$

Nielsen's expression linking the nucleation rate to the total number concentration was extended by Mohanty et al. (1990) to account for growth controlled by surface integration:

$$\log N_t = K_{N1} - \frac{3}{4} K_{ti2} (\log S)^{-2}. \tag{5}$$

Crystal growth is usually described as a two-step process in which solute molecules are first transported to the crystal surface by diffusion through the boundary layer and are then incorporated into the crystal lattice by surface integration. The fundamental driving force for growth (as well as for nucleation) is the difference in chemical potential between the crystallizing substance in the solution and in the crystal. This difference is written

$$\frac{\Delta \mu}{RT} = \ln \frac{a}{a^*} = \ln \frac{\gamma \cdot c}{\gamma^* c^*} \tag{6}$$

for nonelectrolytes. It is often assumed that the activity coefficient ratio is close to unity, and that $\ln S$ can be used to describe the driving force. It is also quite common to use $\Delta c = c - c^*$ even though this is only acceptable at low supersaturation, that is, when $\ln(a/a^*) < 0.1$ (Söhnel and Garside, 1992).

Detailed models of the surface integration step have been developed. At higher supersaturation, growth by two-dimensional nucleation is likely to dominate, and is described by

$$G = C_1 f(S) \exp\left(\frac{C_2}{\ln S}\right). \tag{7}$$

Different expressions for $f(S)$ have been proposed in the literature, for example (Nielsen, 1984),

$$f(S) = S^{7/6} (S-1)^{2/3} \ln S^{1/6}. \tag{8}$$

Surface integration models describe the growth of a single crystal face. If the shape is constant, which is a common assumption, there is a constant relation between the growth rates of the different faces, and it is assumed that the entire growth of the crystal can be represented by a face growth type of equation. This is a simplification since different faces can grow by different mechanisms.

The rate of mass transfer through the boundary layer to the interface is usually described by

$$G_d = k_d \frac{M_c}{\rho_c}(c - c_i). \tag{9}$$

Armenante and Kirwan (1989) examined the contributions of convection and molecular diffusion to the mass transfer to microparticles and proposed the following correlation for the mass-transfer coefficient k_d:

$$Sh = 2 + 0.52\, Re^{0.52} Sc^{1/3}. \tag{10}$$

As the size of the particles or the rate of agitation decreases, the relative velocity between particle and fluid decreases, and the second term on the righthand side becomes negligible.

The relative importance of the boundary-layer diffusion resistance changes with particle size and supersaturation, and it is often difficult to clearly establish which surface integration mechanism is in control. Hence, the use of a simpler power law, such as

$$G = k_g (\ln S)^g, \tag{11}$$

(Mahajan and Kirwan, 1994) can be justified. Over a limited range of supersaturation, it has been found that the simple equation

$$G = k_g (c - c^*)^g \tag{12}$$

provides a good description of the overall growth rate.

It has been shown that the growth rate may vary among crystals of equal size in the same solution (Söhnel and Garside, 1992). However, growth-rate dispersion is usually not acknowledged in reaction crystallization studies. Growth-rate dispersion is generally viewed as resulting from variations in the number and nature of dislocations on the crystal surface. Consequently, it would only be observable when crystals grow under surface integration control. Two models for growth-rate dispersion have been proposed: the random-fluctuation (RF) model and the constant-crystal-growth (CCG) model. The second is applied in this work. It is based on the assumption that each crystal is formed with an intrinsic capacity for growth, a growth-rate activity, which remains constant during the crystal's lifetime. Growth-rate dispersion arises if there is a distribution of growth-rate activities within the crystal population.

Experimental Work

Benzoic acid is crystallized by mixing equimolar hydrochloric acid and sodium benzoate solutions in a T-mixer. Reactant concentrations (c_r) ranging from 0.179 M to 0.340 M are investigated. Concentrations and volume flow rates of reactant solutions are equal in each experiment. The product-size distribution is determined.

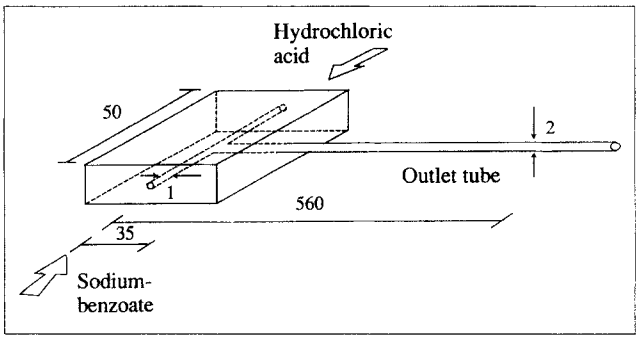

Figure 1. T-mixer with dimensions given in mm.

Apparatus

The reactants are contacted by impingement from opposite directions in a T-coupling, and the mixture is forced into an outlet tube and finally into a sampling beaker. The T-mixing device is shown in Figure 1. The T-block is made of Perspex. The inlet tubes for the reactant solutions have bore diameters of 1 mm and lengths of 22 mm on each side of the mixing point. The outlet tube, which is made of glass, has an internal diameter of 2 mm and a length of 560 mm. It is mounted in the T-block up to the mixing point. At the other end of the outlet tube a plastic tube is fitted that leads down into a stirred and thermostated vessel. On each inlet tube, there is an electrically controlled on-off magnet valve. Both valves are opened simultaneously when the electricity is switched on. Perfluoroalkoxy (PFA) SWAGELOK tubing and tube fittings are used for the solutions, and the materials in the valves in contact with the solution are Viton and Kynar. The reactant solutions are stored in 5-L vessels, placed in a thermostated water bath. The materials of the vessels are titanium-palladium alloy for the hydrochloric acid vessel, and titanium for the vessel of the sodium benzoate solution. At the beginning of the experiment, the pressure in the storage vessels is raised. When the magnetic valves open, the pressure drives the reactants into the T-coupling. The vessels are gradually drained during the experiment. To limit the pressure decrease due to volume expansion, the reactant vessels are connected to a mutual gas-filled 25-L tank. This tank is in turn connected to a gas-pressure cylinder via a pressure regulator. On the gas side, the tubes are made of reinforced nylon.

Procedures

The reactant solutions are prepared at least one day before the experiment, and stored at 30°C. Concentrated hydrochloric acid is mixed with distilled water and filtered through a 0.2-μm membrane filter at preparation. The sodium benzoate solution is filtered a couple of hours before the experiment. The solutions are poured into each respective 5-L vessel at 30°C and the pressure is raised to an absolute pressure of approximately 0.3 MPa. After each experiment, the T-mixer

is cleaned with concentrated ethanol solution to dissolve remaining benzoic acid. At the start of a new experiment, the outlet tube and the acid side of the T-mixer are filled with hydrochloric acid solution. The tube on the sodium benzoate side is filled with distilled water. By this procedure, air is removed from the system and wall deposition is essentially circumvented. The magnetic valves open simultaneously, and reactant solutions are forced by the pressure through the T-mixer and out into the thermostated vessel. The pressure regulator to the gas-pressure cylinder is open during the experiment to help maintain a constant pressure and constant flow rates. The superficial velocity in the outlet tube is normally 5 m/s (flow rate of 15.7 mL/s). However, in a few experiments velocities down to 1.9 m/s have been investigated.

In most experiments carried out, and in all that are used in the evaluation of kinetics, nucleation takes place in the outlet tube of the T-mixer. The crystals grow in the tube and possibly also during the sampling. Sampling of the T-mixer outlet flow is done after approximately 20 s from the start of the experiment, corresponding to 180 outlet-tube residence volumes. During about 2 s, a sample of approximately 30 mL, that is, 17 residence volumes, is collected into a small beaker, originally containing a drop of dispersant. This sample is treated with ultrasound, and a syringe is used to withdraw a smaller sample. The crystals tend to aggregate during the crystallization. However, the forces are weak and complete disintegration is essentially achieved by the dispersant and ultrasound treatment. The particle-size distribution is determined by electrosensing zone measurements (Elzone 180 XY). The measuring tube with an orifice diameter of 38 μm is normally used, which in practice covers particle sizes ranging from 1.23 μm to 19.4 μm. In a few analyses where larger particles are present, a tube with an orifice diameter of 95 μm is used, covering the range 2.35 to 34.5 μm. The sample is weighed and mixed with a weighed amount of electrolyte solution in the jacketed, thermostated measuring vessel of the instrument. In all, about 0.2–0.5 g of sample is added to about 110–130 g of electrolyte. The electrolyte solution contains 1 wt. % of NaCl, and has been saturated with benzoic acid at 30°C, filtered through a 0.2 μm membrane filter, and is slightly undercooled (see below) during the size distribution determination.

The size distribution is determined within a minute from the original sampling of the suspension coming out of the T-mixer, and data are transferred to a computer for storage. After approximately two additional minutes a new analysis of the same solution in the jacketed measuring beaker is carried out in order to examine the stability of the size distribution during determination. It turns out that the crystals dissolve if the electrolyte solution is only just saturated with benzoic acid. The total volume of the crystals is considerably lower in the second of two successive analyses. The dissolution seems to be due to a relatively rapid aging of the crystals. By trial and error, it was found that the electrolyte must be supersaturated by approximately 0.5–0.7°C undercooling to obtain a stable size distribution, so this procedure was used in the present study. Crystals grow in the electrolyte at higher undercooling, which results in an increased total volume of solid phase. The appropriate undercooling depends on the initial supersaturation in the T-mixer experiment. To study the aging behavior further, an experimental study has been carried out and is currently being analyzed. The work is to be reported in a later article. Samples are also examined by microscopy. The induction time is estimated from visual observations of the precipitation front in the outlet tube. The superficial velocity is calibrated from recordings of time vs. weighed amount of fluid coming out of the tube.

Table 1 presents the experimental program, and summarizes the results. Several experiments have been repeated once or twice. In those cases, the table specifies a range of 95% confidence for the resulting parameter value. The reproducibility of the experiments is further shown in Figure 2, for $S_0 = 4.1$. Product population density distributions of three different experiments carried out at identical conditions are compared. The total crystals mass is calculated from the measured size distributions and is compared with the mass

Table 1. Experimental Conditions and Results

Reactant Conc. [mol/L]	Initial Supersat. Ratio	Linear Vel. [m/s]	No. of Exp.	Total No. Conc. [No./m^3]	No. Median [μm]	L_{43} [μm]	Induct. Time [ms]
0.179	2.8	5.1*	1	—	—	—	2500**
0.222	3.5	5.2*	1	3.3×10^{13}	5.5	9.3	470**
0.234	3.5	5.4*	2	$(1.2\pm0.1)\times10^{14}$	3.9 ± 0.0	6.8 ± 0.2	330**
0.246	3.9	5.3*	1	1.5×10^{14}	3.8	6.2	—
		1.9	2	$(1.4\pm0.0)\times10^{14}$	3.9 ± 0.0	6.6 ± 0.0	140
0.258	4.1	5.2	3	$(1.9\pm0.1)\times10^{14}$	3.3 ± 0.1	6.0 ± 0.2	60
0.270	4.3	5.3	1	2.7×10^{14}	3.3	5.5	40
0.276	4.4	5.5	2	$(2.8\pm0.1)\times10^{14}$	3.2 ± 0.1	5.4 ± 0.1	20
0.282	4.5	5.2	1	$3.4\cdot10^{14}$	3.1	4.9	7
0.288	4.6	5.5	2	$(4.6\pm0.1)\times10^{14}$	2.9 ± 0.1	4.5 ± 0.1	3
		3.3	1	4.5×10^{14}	3.0	4.7	—
0.293	4.7	5.5	2	$(4.9\pm0.3)\times10^{14}$	2.9 ± 0.1	4.3 ± 0.2	2
0.300	4.8	5.5	1	5.6×10^{14}	2.9	4.3	1
0.305	4.9	5.5	2	$(6.3\pm0.2)\times10^{14}$	2.7 ± 0.0	3.9 ± 0.1	0.5
0.317	5.1	5.5	2	$(6.7\pm0.0)\times10^{14}$	2.7 ± 0.0	3.9 ± 0.0	—
0.340	5.5	5.5	2	$(8.6\pm0.0)\times10^{14}$	2.4 ± 0.0	3.5 ± 0.0	—

*Sampling from thermostated vessel.
**Time for the precipitation front to reach the T-mixing point after the flow stops.

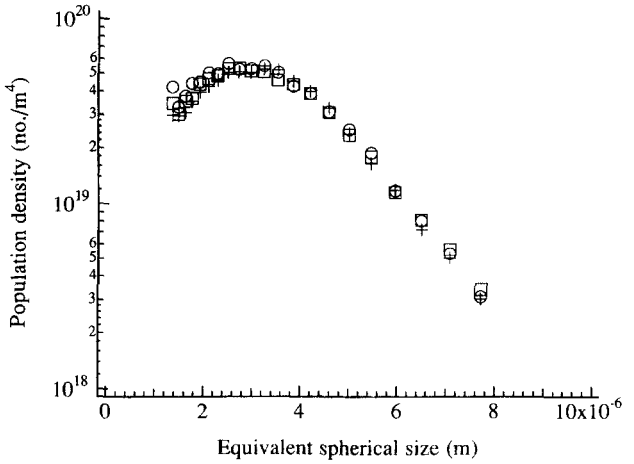

Figure 2. Reproducibility of population density distributions at $S_0 = 4.1$.

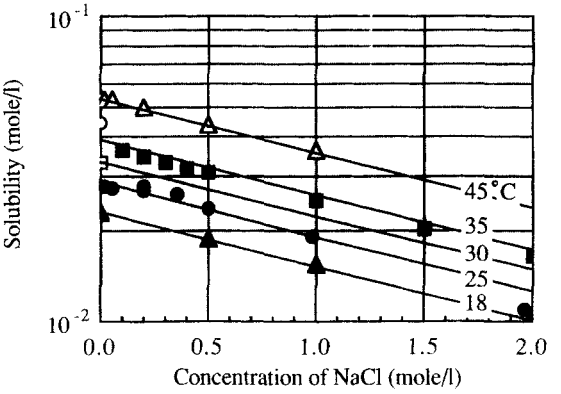

Figure 3. Solubility of benzoic acid.

corresponding to complete consumption of the supersaturation. The deviations range stochastically from 0 to 8%. Thus essentially all supersaturation is consumed in the experiments.

Solubility

The solubility of benzoic acid in pure aqueous solutions and in the presence of sodium chloride has been measured by Ward and Cooper (1930), Seidell (1940), Bourgoin (1878), Larsson (1930a,b), Herz and Hiebenthal (1928), Hoffman and Langbeck (1905), and Goeller and Osol (1937). A multiple regression analysis of data in the literature (including 37 data points) has been performed in the temperature range 18 to 45°C, and for sodium chloride concentrations from 0 to 2 M. The solubility of benzoic acid is described by

$$\log c^* = -5.6329 + 0.0137T - 0.1771 c_{\mathrm{NaCl}}, \qquad (13)$$

in which c^* and c_{NaCl} are in moles/L, and T in degrees kelvin. The R-squared test value for this equation is 0.998. In Figure 3, the equation is plotted as solubility vs. the concentration of sodium chloride at different temperatures and is compared with the underlying experimental data.

Results of experiments

The experimental program and results are shown in Table 1. The initial supersaturation ratio S_0 is calculated from the stoichiometric reaction of equimolar solutions

$$S_0 = \frac{1}{c^*}\frac{c_r}{2}, \qquad (14)$$

and ranges from 2.8 to 5.5. The table contains the superficial velocity in the outlet tube, the induction time, the total number of detected product crystals per unit volume, the number median-size and the corresponding weight mean size, which is calculated as

$$L_{43} = \frac{\Sigma N_i L_i^4}{\Sigma N_i L_i^3}, \qquad (15)$$

where N_i is the number of particles in detection size interval i of the instrument, and L_i is the arithmetic mean size of the interval.

In Figure 4, the classic representation of total crystal number concentration and induction time vs. initial supersaturation ratio is shown. The curves are nonlinear, which indicates that different mechanisms dominate in different regions (Nielsen, 1969; Mohanty et al., 1990). Both curves exhibit a decreasing slope at decreasing supersaturation. There is a reasonably linear part in both curves at higher supersaturation, that is, lower $(\log S_0)^{-2}$. Above $S_0 = 4.0$, the total crystal number is larger than 10^{14} no./m^3, which is the value that is usually observed for heterogeneous nucleation (Nielsen and Söhnel, 1971). Hence, a reasonable interpretation is that homogeneous primary nucleation dominates at high supersaturation, and that a mechanism transition takes place at lower supersaturation. The data of the linear high supersaturation region are correlated by

$$\log t_{\mathrm{ind}} = -13.53 + 4.87\,(\log S_0)^{-2} \qquad (16)$$

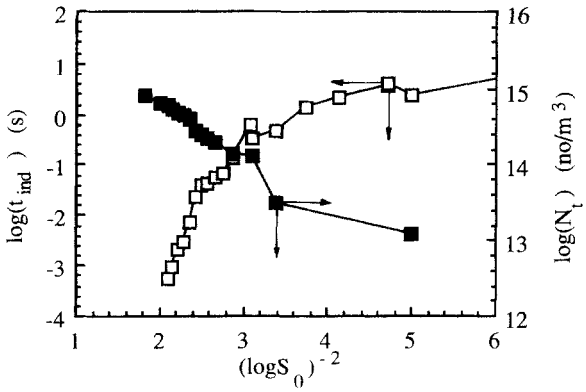

Figure 4. Experimental induction time and total product number concentration.

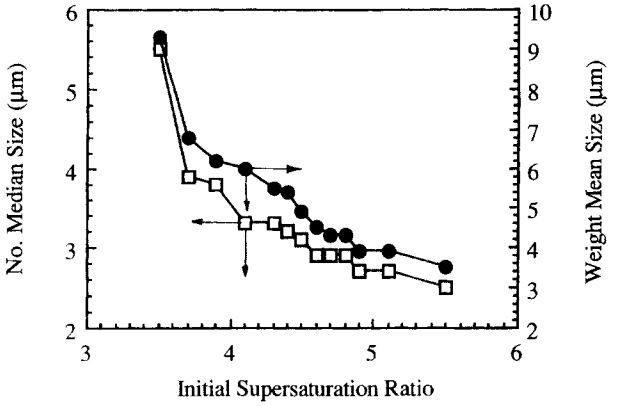

Figure 5. Experimental number median size and weight mean size.

$$\log N_t = 16.81 - 0.955(\log S_0)^{-2}. \qquad (17)$$

The influence of the initial supersaturation on the product crystal size is shown in Figure 5. The number median size and the weight mean size decrease with increasing initial supersaturation. Examples of experimental product-size distributions are shown in Figure 6. For all initial supersaturation studied, a maximum in the population-density distribution is found within the range of detection, that is, for particles larger than 1.23 μm.

At the initial supersaturations exceeding 4.9, precipitation is observed at the mixing point of the T. Above 4.9, the influence of supersaturation on product population and mass-density distributions decreases. This reduced influence can also be seen in the evolution of the mean size (Figure 5). We conclude that at initial supersaturations higher than 4.9, it cannot safely be assumed that the solution is well mixed before nucleation commences. At a supersaturation lower than 3.9, formation of crystals cannot be observed in the outlet tube, but starts in the sampling vessel. Product population-density distributions continue to flatten out, that is, the number of small crystals decreases and the number of larger crystals increases, as the supersaturation decreases.

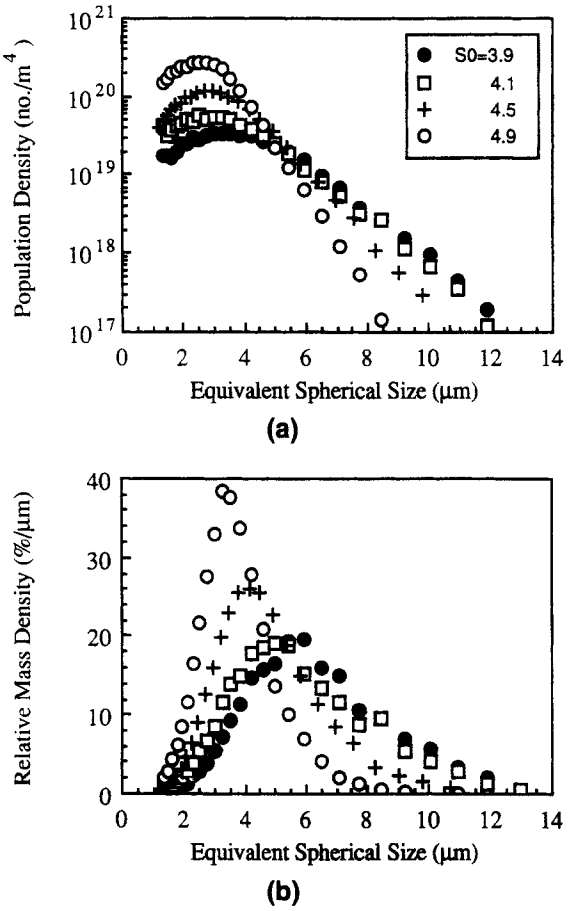

Figure 6. (a) Population density, and (b) mass density distributions at different supersaturations.

Figure 7 shows the different crystal shapes that are obtained from different initial supersaturations. Dendrite-shaped crystals are observed at the lowest studied initial supersaturation ($S_0 = 2.8$), and they decrease in occurrence up to about $S_0 = 3.9$. The left photograph shows a dendrite-shaped crystal from an experiment with an initial supersatu-

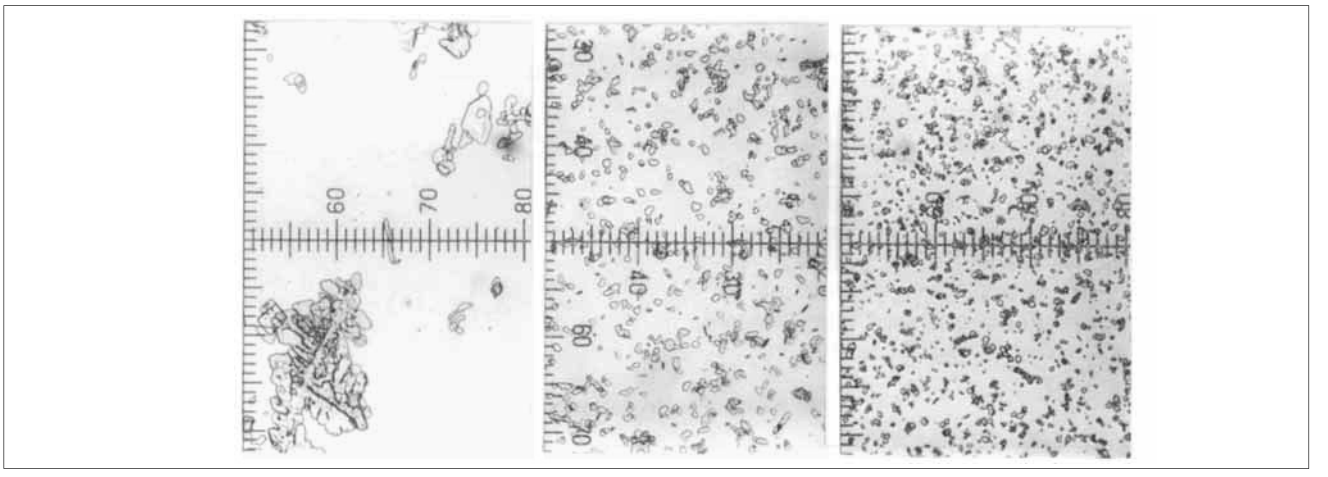

Figure 7. Product crystals obtained at, from left to right, $S_0 = 3.5$, 4.3, and 4.9.

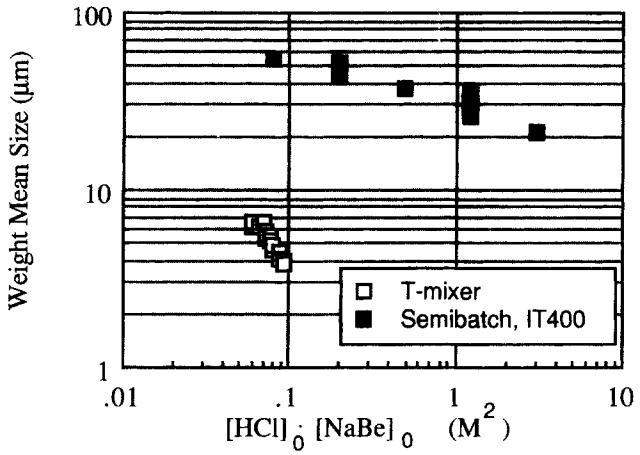

Figure 8. Comparison of product weight mean size from the T-mixer and a semibatch process.

ration of 3.5. At higher supersaturation dendrites are not observed, but the crystal shape is irregular, as may be seen in the middle photograph where $S_0 = 4.3$. At even higher supersaturation, $S_0 = 4.9$, the crystals are smaller with rounded corners.

The product mean size decreases with increasing initial supersaturation. In comparison to semibatch stirred-vessel processing (Åslund and Rasmuson, 1992), much smaller crystals are obtained in the T-mixer, as is shown in Figure 8. In semibatch agitated-tank processing, the supersaturation generated at the feed point can be diluted by further mixing into the bulk solution. Alternatively, small nuclei generated at the feed point may dissolve in the bulk where the supersaturation is much lower. In the T-mixer, the reactants are efficiently mixed, and no dilution or dissolution in a bulk solution is possible. In addition, the reactant concentration in the bulk solution in the semibatch process gradually decreases and agitation brings a gradually increasing concentration of crystals back to the feed point. Hence, the feed-point nucleation gradually decreases, favoring growth of crystals that are already present in the tank.

Evaluation of Kinetics

Nucleation and growth kinetics are estimated from experimentally determined size distributions and known initial supersaturations. Only experiments with an initial supersaturation ratio in the range 4.1 to 4.9 are included. At lower supersaturation, the crystal shape is quite different. At higher supersaturation, where the induction time for nucleation is very short, the mixing time in the T-mixer is no longer sufficiently short to ensure that the influence of mixing can be ignored. A population-balance model over the experiment is developed and kinetics are determined by nonlinear optimization. The results from all selected experiments are included in the optimization, and the difference between simulated and experimental size distributions is minimized.

Model

The T-mixer experiment is modeled as an isothermal plug-flow tube reactor followed by a perfectly mixed semibatch reactor, the latter representing the beaker in which samples are collected. The following assumptions are made: (1) perfect mixing of the reactants is obtained instantaneously in the T-mixer; (2) the chemical reaction is instantaneous; (3) benzoic acid is not dissociated and crystallizes as a molecule; (4) crystals are born at the critical size according to the Gibb-Thomson equation; (5) the crystal shape is constant; (6) breakage and agglomeration are negligible; (7) hydrodynamic axial dispersion in the T-mixer is negligible; (8) the semibatch reactor is perfectly mixed, and (9) no nucleation takes place in the semibatch crystallizer.

If growth dispersion is negligible, the population balance for a plug-flow crystallizer with constant superficial velocity u_z is written (Randolph and White, 1977)

$$u_z \frac{\partial n}{\partial z} + G \frac{\partial n}{\partial L} = 0, \tag{18}$$

and the population balance for the well-mixed semibatch crystallizer is described by

$$\frac{\partial n}{\partial t} + G \frac{\partial n}{\partial L} + \frac{n}{V} \frac{dV}{dt} - \frac{Q n_{\text{feed}}}{V} = 0. \tag{19}$$

In order to account for growth dispersion, the CCG-model is adopted (Ramanarayanan et al., 1984). Each crystal is born with a growth-rate activity K_g, which remains constant during the crystal's lifetime, independent of size and supersaturation. However, there is a distribution of growth-rate activities within a crystal population, which results in growth-rate dispersion. As the population grows, an initially monosized crystal size distribution will gradually attain the same functional form as the distribution of growth-rate activities (Bohlin and Rasmuson, 1992).

The growth rate of a given crystal is expressed by

$$G = K_g D(c, c^*), \tag{20}$$

where $D(c, c^*)$ is the driving-force function for growth (Klug and Pigford, 1989). The distribution of growth-rate activities is given by the distribution function

$$P_g = P_g\left(\bar{K}_g, \sigma_g, K_g\right). \tag{21}$$

Using this approach and transforming the size scale of the outlet tube into time scale, $t = z/u_z$, the population balance for the T-mixer is written for each K_g:

$$\frac{\partial n(L, t, K_g)}{\partial t} + K_g D(c, c^*) \frac{\partial n(L, t, K_g)}{\partial L} = 0, \tag{22}$$

and similarly for the semibatch crystallizer:

$$\frac{\partial n}{\partial t} + K_g D(c, c^*) \frac{\partial n}{\partial L} + \frac{n}{V} \frac{dV}{dt} - \frac{Q n_{\text{feed}}}{V} = 0. \tag{23}$$

The total population density at each crystal size is obtained by integration over all growth-rate activities:

$$n(L, t) = \int_0^\infty n(L, t, K_g)\, dK_g. \tag{24}$$

The population balance is transformed into a system of ordinary differential equations using the method of characteristics (Randolph and Larson, 1988). The generation of crystals in the T-mixer is discretized into pulses, forming subpopulations of particles, and the subpopulations are traced as they grow along the size axis. The total residence time is divided into time steps. During at time step, the supersaturation is assumed to be constant, and nuclei born in that time step form a new subpopulation that is monosized initially.

The number of crystals in the subpopulation that is generated in the time interval i is calculated by integration of the nucleation rate over the time interval

$$N_i = \int_{t_i}^{t_{i+1}} B_p dt, \tag{25}$$

where t_i is the birth time of the subpopulation. The initial size of the crystals is the critical size according to the Gibbs-Thomson relation (Ostwald, 1900)

$$L_{i,0} = \frac{2k_a}{3k_v} \frac{v_m \gamma_s}{kT \ln S_i}. \tag{26}$$

The moment analysis developed by Klug and Pigford (1989) is used to trace the evolution of the size-distribution moments as crystals grow. The moments are calculated from the initial moments of the size distribution m_L, the moments of the growth-activity distribution m_g, and the transformed time Θ_{ij} (Klug and Pigford, 1989; Bohlin and Rasmuson, 1992)

$$m^{ij}_{Lk}(\Theta_{ij}) = \sum_{r=0}^{r=k} \binom{k}{r} m^{ij}_{L(k-r)}(\Theta_{ij}=0) \cdot m^{i}_{g,r} \cdot (\Theta_{ij})^r \qquad k = 0, 1, 2, \ldots. \tag{27}$$

The transformed time is defined as the integral of the driving-force function for growth over the total time of growth. For each subpopulation, the following expression is obtained in the T-mixer:

$$\Theta_{ij} = \int_{t_i}^{t} D(c, c^*)\, dt, \tag{28}$$

and in the semibatch reactor:

$$\Theta_{ij} = \int_{t_i}^{t_{T\text{mixer}}} D(c, c^*) dt + \int_{t_j}^{t} D(c, c^*)\, dt, \tag{29}$$

with $t_{T\text{mixer}}$ being the residence time in the T-mixer. The initial moments of subpopulation i, born at the critical size L_{i0}, are calculated as

$$m_{Lri}(0) = N_i (L_{i0})^r \qquad r = 0, 1, 2.... \tag{30}$$

By calculating the total amount of crystallized material in each time interval, the population balance is coupled to the supersaturation balance. In the plug-flow reactor, benzoic acid is consumed by nucleation and crystal growth. If we assume that the particle-free volume can be approximated with the total volume, we obtain

$$\frac{dc}{dt} = -\frac{dM_T}{dt}. \tag{31}$$

In the semibatch reactor, there is over a period of time (the sampling time) a continuous supply of crystals and dissolved benzoic acid from the T-mixer. The total mass balance over benzoic acid is expressed as

$$\frac{d[c(t)V(t)]}{dt} = -\frac{d[M_T(t)V(t)]}{dt} + Q(c_{\text{feed}} + M_{T,\text{feed}}). \tag{32}$$

By assuming constant volumetric flow in the T-mixer, the mass balance can be rewritten as

$$\frac{dc}{dt} = -\frac{1}{V}\frac{d\tilde{M}_T}{dt} + \frac{Q}{V}(c_{\text{feed}} - c + M_{T,\text{feed}}), \tag{33}$$

where $\tilde{M}_T$ is the total amount of moles of crystallized benzoic acid in the vessel. The total volume in the semibatch reactor changes with time according to

$$V = V_0 + Qt. \tag{34}$$

The amount of crystallized benzoic acid is calculated from the third moment of the subpopulations as

$$M_T = \frac{\rho_c k_v}{M_c} \sum_{i=1}^{i_{\max}} \sum_{j=1}^{j_{\max}} m_{L3ij}, \tag{35}$$

since the total mass is the sum of the mass of all subpopulations. Because the functional form of a subpopulation is determined by the growth-rate distribution, the size distribution can be constructed from the distribution function P_g. The parameters $\bar{K}_g$ and σ_g are substituted by the mean size $\bar{L}_{ij}$, and the standard deviation σ_L^{ij} of the size distribution, which are determined from the moments of the subpopulations, as described by Randolph and Larson (1988).

To determine the population density at size L, we multiply with the total number of crystals in the population and obtain

$$n_{ij}(L) = N_{ij} P_L\left(\bar{L}_{ij}, \sigma_L^{ij}, L\right). \tag{36}$$

The total population density is the sum of the population densities of all subpopulations:

$$n(L) = \sum_{i=1}^{i_{\max}} \sum_{j=1}^{j_{\max}} n_{ij}(L). \tag{37}$$

The growth-rate activity distribution is assumed to be log-normal. The log-normal distribution has a shape that corresponds to the shape of the experimental size distribution, and it does not allow negative growth rates. Previous work at our laboratory has shown this function to be useful in describing growth-rate dispersion of secondary nuclei, and to be more computationally efficient than the gamma distribution. The

log-normal distribution function is described by

$$P_g = \frac{1}{\sqrt{2\pi}\ln\sigma_g'}\exp\left[-\frac{\left(\ln K_g - \ln \bar{K}_g'\right)^2}{2\ln^2\sigma_g'}\right], \quad (38)$$

where $\bar{K}_g'$ is the geometric mean and σ_g' is the standard deviation of $K_g/\bar{K}_g'$ (Randolph and Larson, 1988):

$$\bar{K}_g' = \frac{\bar{K}_g}{\exp\left(0.5\ln^2\sigma_g'\right)}, \quad (39)$$

and

$$\ln\sigma_g = \sqrt{\ln\left(CV_g^2+1\right)}. \quad (40)$$

The coefficient of variation CV_g for the growth-activity distribution of each subpopulation is determined by the supersaturation at the time when the population is born:

$$CV_g = CV_{gk}(c-c^*)^{CV_{gc}}. \quad (41)$$

The rth moment of the growth-activity distribution is calculated as (Randolph and Larson, 1988)

$$m_{gr} = K_g^{r\prime}\exp\left(0.5r^2\ln^2\sigma_g'\right) \qquad r = 0, 1, 2.... \quad (42)$$

When the log-normal distribution is inserted into Eq. 36, the following expression is obtained for the size distribution of the ith subpopulation:

$$n_i(L) = N_{ij}\frac{1}{\sqrt{2\pi}\ln\sigma_L'^{(ij)}}\frac{1}{(L-L_{i0})}\exp\left(-\frac{\left[\ln(L-L_{i0})-\ln\bar{L}_{ij}'\right]^2}{2\ln^2\sigma_L'^{(ij)}}\right), \quad (43)$$

with

$$\bar{L}_{ij}' = \frac{\bar{L}_{ij}-L_{i0}}{\exp\left(0.5\ln^2\sigma_L'^{(ij)}\right)}, \quad (44)$$

$$\ln\sigma_L'^{(ij)} = \sqrt{\ln\left[\left(\frac{\sigma_L^{(ij)}}{\bar{L}_{ij}-L_{i0}}\right)+1\right]}. \quad (45)$$

Before the model can be implemented, expressions for nucleation and growth must be specified. The primary nucleation rate is described by

$$B_p = K_{p1}\exp\left(-\frac{K_{p2}}{\ln^2 S}\right). \quad (46)$$

The driving-force function, $D(c, c^*)$, in Eq. 20 is described by either a normal power law (Eq. 47), a power law with a logarithmic driving force (Eq. 48), or a two-dimensional nucleation model (Eq. 49).

$$D(c,c^*) = (c-c^*)^g \quad (47)$$

$$D(c,c^*) = (\ln S)^g \quad (48)$$

$$D(c,c^*) = S^{7/6}(S-1)^{2/3}\ln S^{1/6}\exp\left(-\frac{g}{\ln S}\right). \quad (49)$$

The simulation begins with a simulation of the crystallization in the T-mixer in order to determine the size distribution of the crystals in the feed to the semibatch reactor. It then proceeds to trace the evolution of the crystal-size distribution as the crystals continue to grow in the semibatch reactor. The subpopulations keep their identity as they move down the outlet tube and into the semibatch reactor.

The system of equations is solved using Euler's method. In the simulation of the T-mixer, Eqs. 25 and 28 give the nucleation rate and the transformed time. Equation 27 is used to calculate the change in subpopulation moments and crystal mass. The crystal mass is inserted into Eq. 31 to determine the change in solute concentration. In the simulation of the semibatch reactor, Eq. 33 is used instead of Eq. 31 to determine the change in supersaturation. A time step of 0.2 ms is used in the T-mixer. A further decrease in the time step does not significantly influence the solution. The time step in the semibatch reactor is initially 0.2 ms, and is gradually increased to 96 ms.

Method of parameter estimation

The parameters of the model are determined by fitting simulated size distributions to experimental data. The difference between the experimental and simulated population density distributions is minimized in a nonlinear optimization. The nucleation parameters K_{p1} and K_{p2}, the growth parameters $\bar{K}_g$ and g, and the growth dispersion parameters CV_{gk} and CV_{gc} are determined in the optimization.

Two different optimization methods have been used. The Gauss-Newton method uses the Jacobian in the determination of the search direction, resulting in faster and more reliable convergence (Gill et al., 1981). The calculated Jacobian also allows us to estimate the confidence intervals of the parameters from the covariance matrix, as suggested by Fletcher (1987). However, for models that do not include growth-rate dispersion, the simplex method had to be used instead. The simplex method uses function evaluations to determine the search direction, and is more robust when the objective function has many discontinuities. Both methods are implemented in the Matlab Optimization Toolbox (The Mathworks, Inc., 24 Prime Park Way, Natick, MA 01760-1500, USA). The simulation program is written in Fortran, and it is compiled to a mex-file which is called by the Matlab optimization routine. This construction allows run times of around 1.5 min for a complete simulation of 14 experiments, on a Pentium II 450 MHz. An optimization usually takes up to 2 h.

Experimental data consist of initial supersaturations and final population-density distributions discretized into 21 size classes between 1.2 and 7.7 μm. Each optimization includes 14 experiments with 8 different initial supersaturation ratios ranging from 4.1 to 4.9.

Simulated data consist of the population densities predicted by the model at the mean size of each size class in the

Table 2. Estimated Parameter Values and Corresponding Value of the Objective Function

$D(c, c^*)$	K_{p1}	K_{p2}	$\bar{K}_g$	g	CV_{gk}	CV_{gc}	Σ
Normal power law, Eq. 47	$(3.0\pm1.3)10^{19}$	18.6 ± 0.72	$(2.4\pm2.9)10^{-9}$	2.1 ± 0.29	3.8 ± 17	0.6 ± 0.9	6.6
Log. power law, Eq. 48	$(1.7\pm0.7)10^{19}$	17.5 ± 0.68	$(1.4\pm0.17)10^{-5}$	2.9 ± 0.46	1.5 ± 16	0.38 ± 1.0	6.5
2-D nucleation, Eq. 49	$(2.4\pm0.7)10^{19}$	18.2 ± 0.56	$(5.4\pm1.8)10^{-6}$	0.62 ± 0.3	2.9 ± 26	0.52 ± 0.9	6.5

experimental data. The residual is calculated as the relative difference between experimental and simulated population densities for size class k and experiment l:

$$R_{kl} = \frac{n_{\text{sim}} - n_{\text{exp}}}{n_{\text{exp}}}. \tag{50}$$

This formulation ensures that size intervals with large numbers of crystals are not too strongly weighed in the calculation of the objective function.

If the starting point is located far from an optimum, the residual expression in Eq. 50 cannot be used. Instead the following logarithmic residual is used:

$$R_{kl} = \ln(n_{\text{sim}}) - \ln(n_{\text{exp}}). \tag{51}$$

The objective function is defined as the sum of squares of the residuals:

$$F = \sum_{k=1}^{k_{\max}} \sum_{l=1}^{l_{\max}} R_{kl}^2. \tag{52}$$

To obtain an efficient optimization, the parameters, K_{p1}, $\bar{K}_g$, and CV_{gk} are scaled nonlinearly in the following manner (Fletcher, 1991)

$$x_{\text{new}} = \ln x_{\text{old}}. \tag{53}$$

Linear scaling has also been used, but it results in slower convergence and in optimizations that are more prone to diverge.

In the optimizations, different initial parameter values have been used. Depending on the starting point, different local minima may be found, and in some cases the optimization enters nonstable areas that cause it to diverge. Optimal parameter values are evaluated further by running simulations to assess the evolution of different variables, such as growth and nucleation rates.

Results of parameter estimation

The results of the parameter estimation using the different growth models are summarized in Table 2 together with the corresponding 95% confidence intervals for the estimates. The choice of growth model does not have a strong influence on the results. Growth-parameter values change, but the other parameters are essentially unchanged. If the parameters are used for simulation of the experiments, the evolution of supersaturation, growth rate, and crystal size are quite similar regardless of growth model. Clearly different models can be used to describe the same behavior. Results are presented and analyzed below for the normal power-law equation.

The residuals at the optimum are plotted versus crystal size and vs. initial supersaturation of the experiments in Figure 9. The relative deviations range between -50% and 50%. A

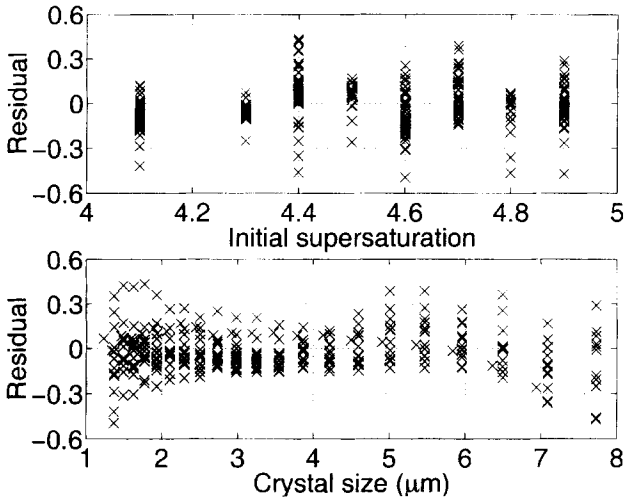

Figure 9. Distribution of relative residuals with initial supersaturation and crystal size.

clear trend would indicate systematic errors. No such trend is seen, although the residuals are not distributed completely evenly. The correlation between simulated and experimental population-density distributions is shown in Figure 10. For clarity, only four of the experiments are shown, but the results are representative for all experiments. Some deviations can be seen, but overall the agreement is quite satisfactory.

The obtained parameter values are used in simulations to evaluate the evolution of supersaturation, nucleation and growth rates, and crystal mean size during the crystallization. The results for an experiment with an initial supersaturation ratio of 4.6 are shown in Figure 11 with data plotted vs. position along the outlet tube. The results are similar for all experiments. The obtained growth rate when only the boundary-layer diffusion resistance is accounted for, that is, when the surface integration resistance is neglected, is also included in the plot. The mass-transfer coefficient is obtained from Eq. 10, and the growth rate is calculated for the total number mean size at each time. To calculate the Reynolds number, Re, the energy dissipation is estimated from the pressure drop. The pressure drop from the containers to atmospheric pressure at the outlet of the T-mixer is $2.3 \cdot 10^5$ N/m^2 when the velocity is 5 m/s in the outlet tube. A pressure drop of approximately 10^5 N/m^2 in the outlet tube leads to a mean energy dissipation rate of about 1 kW/kg according to the following correlation (Calderbank and Moo-Young, 1961):

$$\bar{\epsilon} = \frac{u_z \Delta p}{L_{\text{tube}} \rho_f}, \tag{54}$$

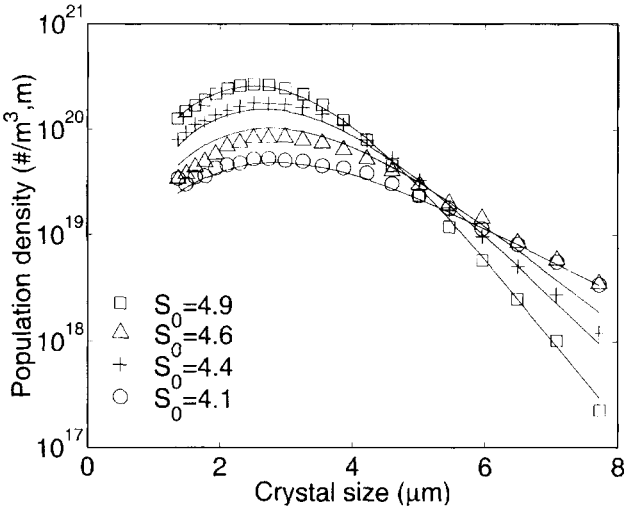

Figure 10. Correlation of optimal simulated population-density distributions to experimental data.

where Δp is the pressure drop and L_{tube} is the length of the outflow tube of the T-mixer.

Figure 12 shows the simulated supersaturation profile for the whole experiment, including the period of sampling in the beaker. At the end of the experiment a supersaturation ratio of 1.3 remains. Figures 13 and 14 compare the simulated total number concentration and the number mean size with the experimental values for particles above the size limit of the measurement technique. For the total number concentration the fit is very good, while the simulated mean size tends to be somewhat lower than the experimental values. Still, the deviation is not strong in view of the scatter in experimental data.

Discussion

Mixing time

In order to capture the influence of supersaturation on the crystallization kinetics, it is very important to have experimental data over the widest possible supersaturation range. Hence, the range of data included in the optimization is not reduced more than is absolutely necessary. The modeling is based on the assumption that the experimental data are uninfluenced by mixing. The mixing time in the T-mixer has not been measured directly, but Mohanty et al. (1988) used a T-mixer of a similar configuration and estimated the mixing time to be 1 ms. Our experimental results indicate that supersaturation has less influence on the population and mass density distribution when the initial supersaturation exceeds 4.9. This coincides with the observation that crystals can be observed at the mixing point of the T. Moreover, the experiment at $S_0 = 4.6$ was carried at two different mixing conditions: $Re = 6000$ and $Re = 10{,}000$, respectively. The results from these two experiments are essentially the same (see Figure 15). Consequently, the influence of mixing is not strong, at least not at this supersaturation level. As described previously the lower supersaturation limit for useful data is set to 4.1, below which a major change in crystal shape can be observed, as is shown in Figure 7. For comparison, optimizations have been carried out with the range of experimental data limited to $4.1 \le S_0 \le 4.6$, that is, the induction time is longer than 3 ms. The optimum obtained is very close to the one reported previously based on the wider range $4.1 \le S_0 \le 4.9$, showing that the experiments with supersaturation ratio between 4.6 and 4.9 follow the same general trend as those below 4.6.

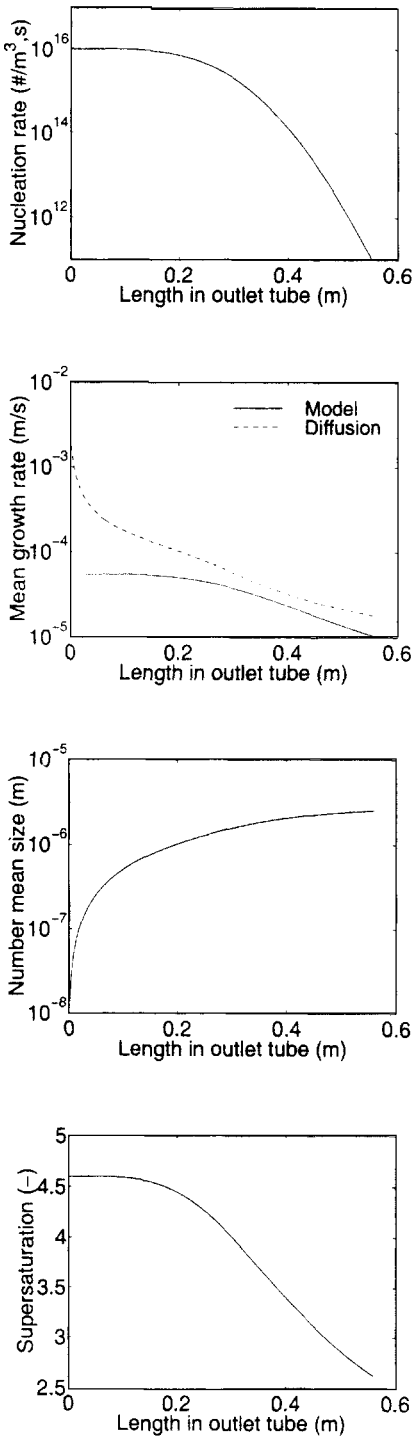

Figure 11. Evolution of nucleation rate, growth rate, number mean size, and supersaturation ratio along the outlet tube of the T-mixer at $S_0 = 4.6$.

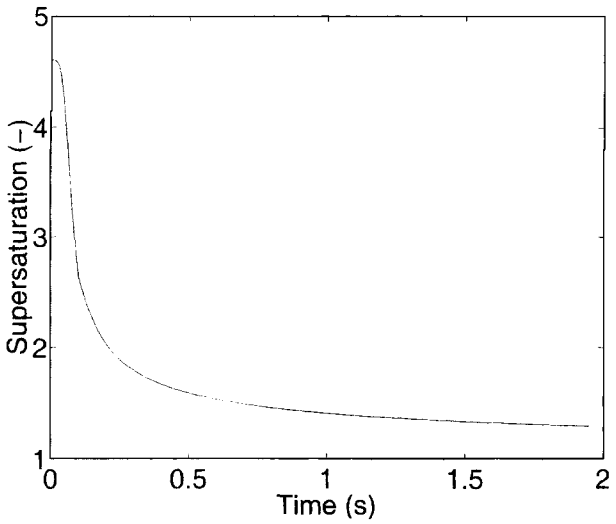

Figure 12. Evolution of the supersaturation during the whole experiment at $S_0 = 4.6$.

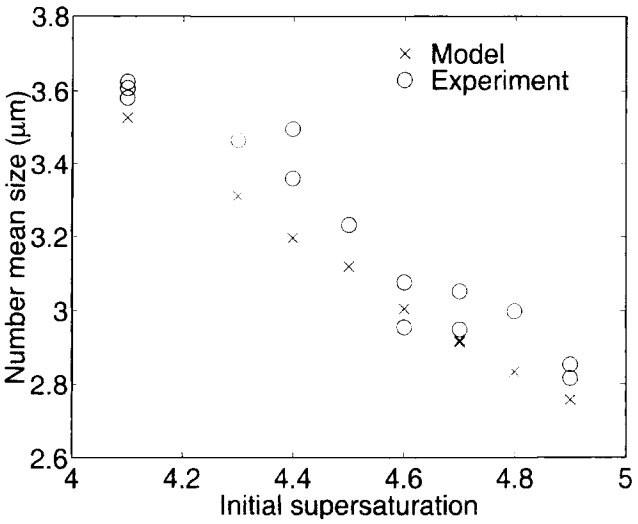

Figure 14. Correlation of simulated number mean size to experimental data.

Model

Before the final model was accepted, four other, increasingly complex, models were evaluated. Either the optimum value of the objective function is significantly higher for these models, because the shape of the simulated size distribution differs significantly from the experimental, or the obtained parameter values are not in agreement with the prevailing view of crystallization kinetics.

The simplest model (model 1) describes a plug-flow tube reactor where growth dispersion is assumed to be negligible. In this case, the population balance in Eq. 18 describes the reactor. However, the crystal size distribution that results from a plug-flow reactor under these conditions decays quite sharply toward zero at larger sizes, as can be seen in Figure 16. The figure shows the result for one value of the initial supersaturation, but the same trend is observed over the whole investigated supersaturation range. The experimental size distribution is broader and has a developed "tail" toward larger sizes, and a significant number of particles are larger than the dominant size. The only mechanism that broadens the size distribution in this simple model is the time distributed nucleation. However, since the supersaturation in this model decays steadily from the initial value, the corresponding product-size distribution has its mode peak close to its maximum size.

Different mechanisms that could broaden the product crystal-size distribution have been examined, and two main possibilities were identified: growth-rate dispersion and further growth in the sampling beaker. Growth-rate dispersion leads naturally to a broadening, but is rarely acknowledged in reaction crystallization studies. Continued growth during the

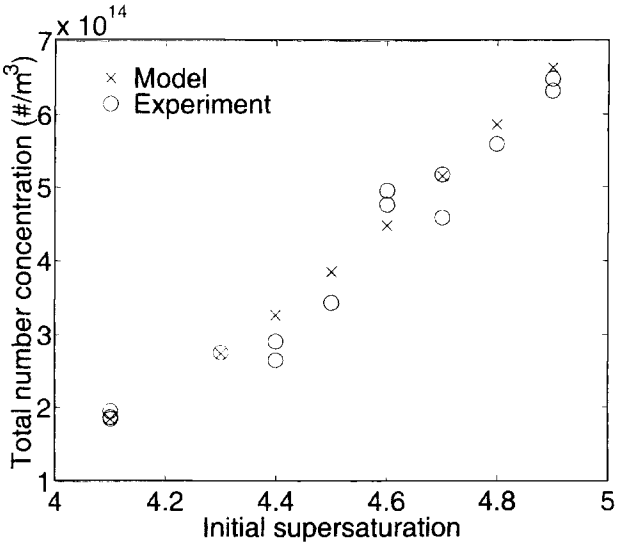

Figure 13. Correlation of simulated total number concentration to experimental data.

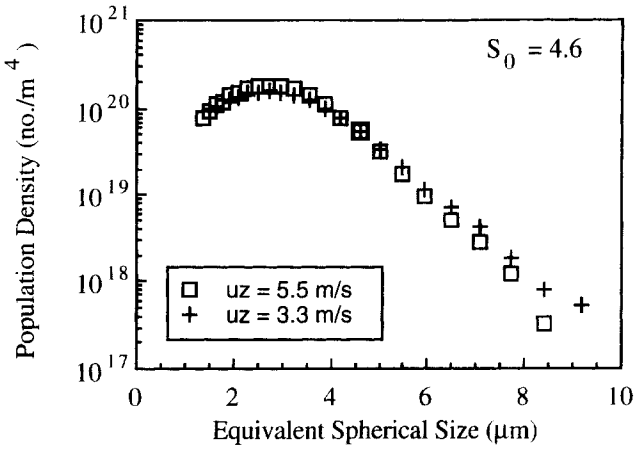

Figure 15. Influence of Reynolds number on the population density distribution at $S_0 = 4.6$.

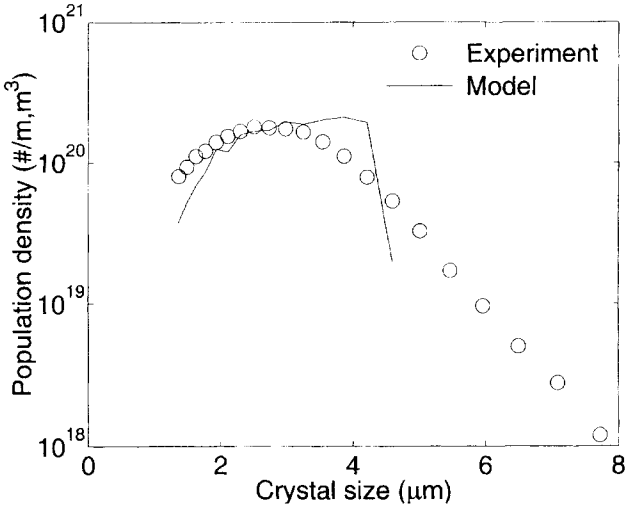

Figure 16. Optimal population density distribution with model 1 at $S_0 = 4.6$, compared to experimental data.

sampling period also gives a broader distribution, since different subpopulations have different residence times in the vessel.

In model 2, a semibatch reactor is attached to the T-mixer in order to account for growth during sampling. Growth-rate dispersion is still neglected. Model 2 gives a better correlation to the experimental data than model 1 (see Figure 17), but significant deviations are still present, and the model is not really capable of describing experimental data. The comparison in Figure 17 is representative of all initial supersaturations investigated.

On the other hand, if growth dispersion is taken into account, but growth during sampling is assumed negligible (model 3), the description of experimental size distributions

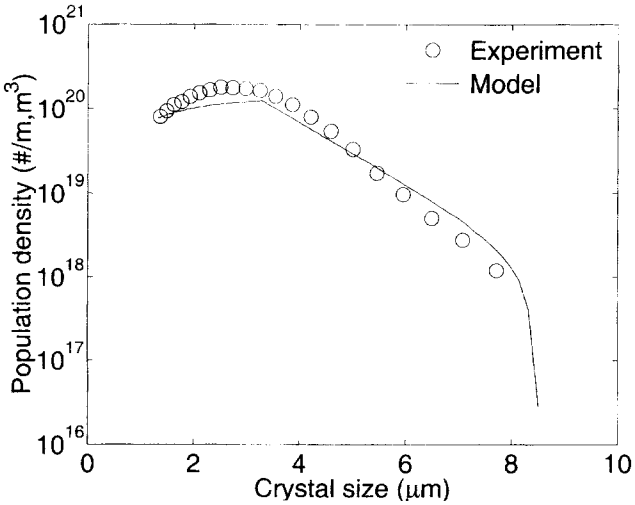

Figure 17. Optimal population density distribution with model 2 at $S_0 = 4.6$, compared to experimental data.

is quite satisfactory (Figure 18). However, if the parameter values that are obtained in the optimization are used in the simulation, the resulting growth rate in the outlet tube of the T-mixer is significantly higher than the growth rate that would result if growth was limited only by boundary-layer mass transfer. The comparison is shown in Figure 19. This is contradictory to the general view of crystal growth as a process, in which diffusion to the crystal surface and integration into the crystal lattice occurs consecutively. The overall growth rate is then limited by the slowest of the two steps, and could not possibly exceed the rate of boundary-layer mass transfer. In the calculation of the boundary-layer mass-transfer rate, the mass-transfer coefficient is obtained from Eq. 10 and is calculated for the number mean size in each time step. We have investigated whether application of another growth-rate equation in this model (instead of the normal power law equation, Eq. 12) may lead to a growth rate that no longer exceeds the boundary-layer mass-transfer rate. Unfortunately, the situation remains the same with other growth equations as well.

If growth-rate dispersion, as well as growth during sampling, is accounted for in the model (model 4), we obtain a satisfactory fit to experimental size-distribution data, as well as realistic growth rates, as shown in Figure 11.

Hydrodynamic backmixing could also be a possible cause for the broadening of the size distribution. Tosun (1988) performed reaction crystallization experiments with barium sulfate in a side-T, and found that the Reynolds number strongly influenced the width of the size distribution. He observed a decrease in the width of the distribution and in the mean diameter when moving from laminar flow ($CV = 0.76$, volume based, at $Re = 880$) to fully turbulent flow ($CV = 0.60$ at $Re = 10{,}000$). Figure 15 shows the size distribution for benzoic acid from two experiments with the same initial supersaturation ($S_0 = 4.6$), but with different superficial velocities. The Reynolds number in the experiments is 10,000 and 6000, respectively. As can be seen in the figure, there is no clear support for the assumption that the product size distribution depends on the Reynolds number. Using the correlation for hydrodynamic dispersion in pipeline flow that was presented by Levenspiel (1972), the coefficient of hydrodynamic dispersion can be estimated to be $5 \cdot 10^{-3}$ m^2/s at our experimental conditions. Assuming that nucleation only occurs at the inlet of the T-mixer tube and that the growth rate is kept constant at $5 \cdot 10^{-5}$ m/s along the tube, axial dispersion causes a spread of ± 0.8 μm around a mean size of 5.5 μm. This broadening effect is not strong enough to explain the broadening observed in the experiments. In this calculation, we neglect the influence of disturbances at the inlet of the tube. However, such disturbances should not be of a magnitude to cause the observed broadening. Therefore, it seems unlikely that hydrodynamic dispersion has more than a minor influence on the crystal-size distribution.

Size-dependent solubility has not been accounted for in the model. The effect is negligible, except for crystals that are close to the critical size, and including size-dependent solubility, would make the model more difficult to solve. Preliminary simulations indicate that the product-size distribution is not greatly affected by size-dependent solubility.

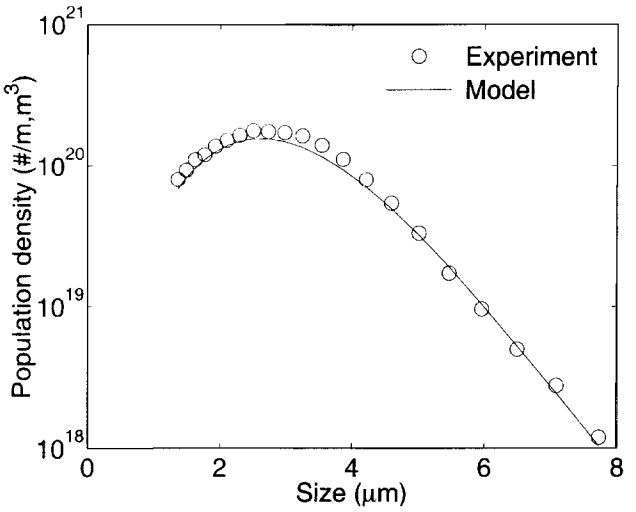

Figure 18. Optimal population density distribution with model 3 at $S_0 = 4.6$, compared to experimental data.

Kinetics

The interfacial energy can be calculated from the nucleation parameter K_{p2} according to

$$K_{p2} = \frac{4k_a^3}{27k_v^2}\left(\frac{M_c}{\rho_c N_{av}}\right)^2\left(\frac{\gamma_s}{kT}\right)^3. \qquad (55)$$

The resulting interfacial energy is 0.015 J/m^2. The same value is obtained regardless of the growth model used. The shape factors of a sphere are used since size is measured as the volume equivalent sphere diameter in the electrosensing zone measurement. The value can be compared to the values that are obtained directly from the experimental induction time and total number concentration. The correlations between these variables and $(\log S_0)^{-2}$ are given in Eqs. 16 and 17. The interface energy is calculated using Eq. 4, resulting in a value of 0.030 for Eq. 16 and 0.015 for Eq. 17. Equation 16 is derived with the assumption that growth is controlled by boundary-layer diffusion. This assumption is not valid for benzoic acid under the conditions of the present work, which might explain the deviation between the interfacial energy values. In addition, the induction time is measured visually in the experiments, making it difficult to obtain accurate measurements. The interfacial energy can also be calculated from the solubility as proposed by Mersmann (1990):

$$\gamma_s = 0.414kT\left(\frac{\rho_c N_{av}}{M_c}\right)^{2/3}\ln\left(\frac{\rho_c}{M_c c^*}\right). \qquad (56)$$

A value of 0.035 J/m^2 is obtained by this equation.

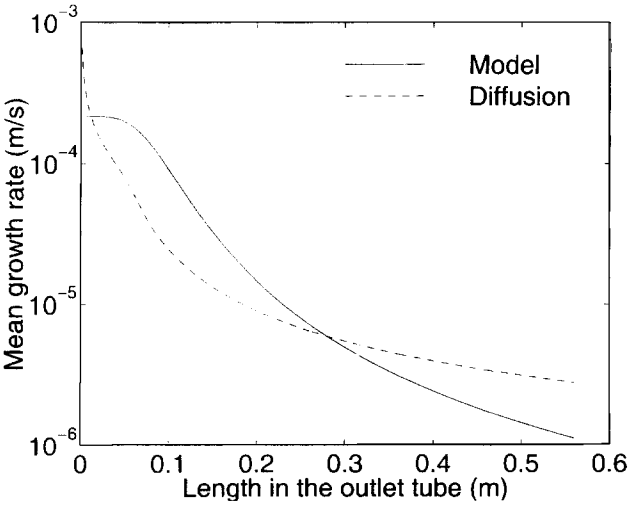

Figure 19. Comparison of simulated growth rate based on model 3 and the corresponding rate of boundary-layer mass transfer.

The value of the preexponential nucleation factor K_{p1} ($\approx 10^{19}$) is low compared to the values that are published in the literature. These values are usually in the 10^{26} to 10^{36} range (Estrin, 1992). Nielsen (1969) evaluated the preexponential factor from the intercept in the plot of the induction time or total number concentration vs. $(\log S_0)^{-2}$. Using the same approach, the preexponential nucleation factor in our work becomes $10^{30.5}$ (no./m^3,s).

The growth exponent in the normal power-law equation is approximately 2, which suggests that surface integration limits the growth rate. This is also supported by the fact that the simulated growth rate is significantly lower than the boundary-layer mass-transfer rate, as shown in Figure 11 for the outlet tube of the T-mixer. The same is true during the semibatch period. Furthermore, growth-rate dispersion is generally viewed as resulting from variations in the surface integration rate. Therefore, the growth rate must necessarily be controlled by the surface integration rate if growth dispersion is to explain the broadening of the product-size distributions. When the power law with a logarithmic driving force is used, the exponent is almost 3.

A growth exponent close to or higher than 2 at fairly high supersaturations also suggests that the surface integration rate is governed by a surface nucleation mechanism rather than a spiral growth mechanism. The latter exhibits an almost linear dependence at higher supersaturation. In addition, when the BCF equation is correlated to our experimental data, the estimated parameters are all more uncertain than for the other models.

For all growth models the dependence of the coefficient of variation on the supersaturation is rather weak. For example, CV_g varies between 0.23 and 0.28 in the high supersaturation range where most particles are formed when the normal power law is used. The CV_g-values are consistent with data in the literature, although those data mostly concern secondary nuclei. Coefficients of variation between 0.17 and 1 have been reported (Bohlin and Rasmuson, 1992). Garside and Ristic (1983) measured values ranging from 0.37 to 0.44 for ADP-crystals formed by primary nucleation at a supersaturation ratio of 1.06.

The ranges of confidence are wide for some of the parameter estimates. This is the case for the growth-rate constant

$\bar{K}_g$ when the normal power law is used, and for the growth dispersion parameters CV_{gk} and CV_{ge} for all growth models. An uncertain estimate results if the value of the objective function is rather insensitive to changes in the parameter, as well as if there is a strong bias between two parameters. The latter seems to be the case for the growth-dispersion parameters. Since most crystals are formed at the beginning of the experiment when supersaturation is high, the CV_g in that part of the simulation has a large influence on the final distribution. As is evident from Eq. 41, several combinations of parameters will give the same value of the coefficient of variation at a certain supersaturation. If the value of exponent CV_{ge} is set to 0 and excluded from the optimization, CV_{gk} (which now equals CV_g) has a value between 0.23 and 0.24, depending on the growth model used. The range of confidence improves dramatically.

The limited supersaturation range and the moderate number of experiments in the optimization may also contribute to the uncertainty of the estimates. However, this is a situation that is somewhat unavoidable in crystallization work. On the other hand, one should also bear in mind that the method for calculating the variance of the estimates is approximate for nonlinear models, since it is based on linear statistics.

Objective function and the optimization

The location of the optimum is, to some extent, affected by the choice of objective function. If the logarithmic residual in Eq. 51 is used in the objective function, the minimum will shift slightly. If the model is less capable of describing data, as is model 2, the influence of the choice of residual is more marked.

The objective function is nonconvex, that is, it has several local minima. As a consequence, different minima can be found when the optimization is started from different initial parameter values. Often the different minima have objective-function values of similar magnitude, and consequently, the purely mathematical–numerical evaluation of the optimum given by the optimization routine is not sufficient for choosing the most reasonable kinetic values. In this work, the estimated parameters are also evaluated by examining the evolution of important crystallization variables, such as supersaturation and growth rate, during the simulation. In some cases, this evaluation is sufficient to eliminate optima that are physically inconsistent; in other cases, there are several minima that all seem realistic. In such cases, a more detailed evaluation must be carried out to determine which optimum is more likely to give the best description of the kinetics of the system.

As an example of this need for a detailed analysis, consider the following situation. Model 4 can be extended to allow for further growth when the sampling period is over. This extension is logical, since the simulation shows that the solution is still supersaturated at the end of the sampling period, and about a minute lapses between the sampling and the actual analysis. If this extended model is furnished with kinetic parameters from model 4 corresponding to the normal power law growth equation, and then is allowed to simulate continued outgrowth in the sampling beaker, the supersaturation decays to a value close to unity, as would be expected. However, if an optimization is carried out with a model that includes this extended growth period, the optimum changes significantly. With the corresponding new optimal parameters, the evolution of the crystallization variables is still consistent, and the objective function value of 6.9 is only slightly higher than the earlier value. The kinetic parameters are compared in Table 3 and the corresponding supersaturation profiles are compared in Figure 20. We can note that the supersaturation ratio does not approach unity in the approach leading to "optimum 2." The reason for this is that the high value of the growth exponent results in a kind of metastable zone for growth. Values of the growth exponent as high as 4.8 are rarely reported, but can be explained within the surface nucleation theory. If this value is correct, in practice we would expect a mechanism transition which would sustain a reasonable growth rate, and in turn lead to a decay of the supersaturation ratio to unity. Within the optimization we do not allow for such a mechanism shift. Growth kinetics are extracted by using data over the whole supersaturation range. It is highly questionable whether a mechanism shift really can be extracted from the data, and a model extended along this line would lead to an undesirable increase in the number of parameters to be determined. Furthermore, the parameters for growth dispersion by the approach leading to optimum 2 result in quite high coefficients of variation for

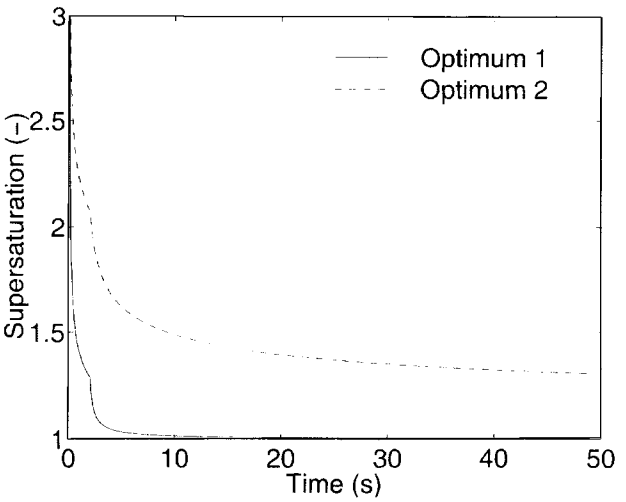

Figure 20. Comparison of simulated supersaturation profiles corresponding to optimum 1 and 2.

The "kink" marks the time when the feed from the T-mixer stops.

Table 3. Kinetic Parameters for Model 4 with (Optimum 2) and without (Optimum 1) Extended Growth Period

	K_{p1}	K_{p2}	$\bar{K}_g$	g	CV_{gk}	CV_{ge}
Optimum 1	$(3.0\pm1.3)10^{19}$	18.6 ± 0.72	$(2.4\pm2.9)10^{-9}$	2.1 ± 0.29	3.8 ± 16.9	0.6 ± 0.94
Optimum 2	$(3.7\pm1.5)10^{20}$	23.4 ± 0.55	$(1.1\pm1.2)10^{-14}$	4.8 ± 0.27	210 ± 368	1.4 ± 0.36

the growth rate. Thus, we find that the approach leading to optimum 1 is more likely to give an adequate description of the kinetics of the system.

Conclusions

Benzoic acid has been crystallized by mixing hydrochloric acid and aqueous sodium benzoate in a T-mixer. At conditions where the reactants are well mixed before nucleation commences, the product weight mean size changes from 3.9 μm to 6.2 μm, when the supersaturation ratio varies between 4.9 and 3.9. Population balance modeling and nonlinear parameter estimation are applied to estimate the kinetics of nucleation and crystal growth.

A model that accounts for primary nucleation, crystal growth, and growth rate dispersion successfully correlate experimental product size distributions. The estimated kinetics are physically reasonable and lead to a physically reasonable description of the entire experiment. The interfacial energy is calculated from the determined nucleation parameter and is found to be 0.015 J/m^2. This value is in good agreement with the value obtained by the traditional method of plotting the measured total number concentration versus the initial supersaturation.

Different growth rate expressions have been evaluated. There are only small differences in the quality of fit, and the nucleation parameter values are almost the same. The exponent of the normal power law growth rate equation has a value of 2.1, which suggests that growth is controlled by surface integration, a conclusion that is further supported by the fact that the calculated growth rate is significantly lower than the boundary layer diffusion rate. It is also consistent with the conclusion that growth rate dispersion significantly contributes to the broadening of size distributions. The exponent changes to 2.9 if the logarithm of the supersaturation ratio is used as driving force. The coefficient of variation of the growth rate distribution depends only weakly on supersaturation. It obtains a value of approximately 0.23 when this dependence is disregarded.

Several models have been examined to obtain an adequate description of the experiments. It is found that the fairly strong tailing of the product size distribution towards larger sizes is difficult to reproduce without introduction of the mechanism of growth rate dispersion.

The objective function is nonconvex with several local minima—a situation which complicates the estimation of kinetics. Often, the mathematical-numerical evaluation given by the optimization routine must be combined with a careful investigation of important variables, such as the growth rate and the supersaturation, during the course of the experiment to identify adequate kinetic parameters. In some cases, clear inconsistencies are discovered. In other cases, the differences may be more subtle and require a more detailed analysis.

Notation

a = activity
B_p = primary nucleation rate, no./m^3, s
C_1, C_2 = constants in Eq. 7
c = solute concentration, mol/m^3
c^* = solubility, mol/m^3
CV_g = coefficient of variation for distribution
CV_{gk}, CV_{gc} = constant and exponent in Eq. 41
$D(c, c^*)$ = driving-force function
D_v = diffusivity, m^2/s
F = objective function
G = crystal growth rate, m/s
G_d = volume diffusion growth rate, m/s
ΔG = Gibbs excess free energy, J
g = exponent in growth-rate expressions
K_{p1}, K_{p2} = primary nucleation-rate parameters
K_{ti1}, K_{ti2}, K_{N1} = parameters in Eqs. 3 and 5
K_g = growth-rate activity
k = Boltzmann constant (1.3805×10^{-23}), J/K
k_a, k_o, k_v = area, perimeter, and volume shape factors
k_d = mass-transfer coefficient, m/s
k_g = growth-rate constant in power laws
L = crystal size, m
L_{tube} = length of T-mixer outflow tube = 0.560 m, m
L_{43} = weight mean size, m
M_c = molar mass, kg/mol
M_T = molar magma density, mol/m^3
m_{gr} = rth moment of growth-rate activity distribution
m_{Lr} = rth moment of size distribution, m^r/m^3
N_{av} = Avogadro's number (6.023×10^{23}), No./mol
N = number of crystals, No./m^3
N_t = total number of crystals per unit volume, No./m^3
n = population density, No./m, m^3
P_g = growth-rate activity distribution function
P_L = size distribution function
Δp = pressure drop, N/m^2
Q = volumetric flow, m^3/s
R = gas constant (= 8,314), J/mol, K
R_{kl} = residual for population kl
Re = Reynolds number = $(\epsilon^{1/3} L^{4/3})/\nu$
S = supersaturation ratio, c/c^*
Sc = Schmidt number = ν/D_v
Sh = Sherwood number = $(k_d L)/D_v$
T = temperature, K
t = time, s
t_{ind} = induction time, s
u_z = velocity, m/s
V = volume, m^3
v_m = molecular volume, m^3
z = position in T-mixer outlet tube, m

Greek letters

ϵ = energy dissipation rate, W/kg
γ = activity coefficient, m^3/mol
γ_s = interfacial surface energy, J/m^2
μ = chemical potential, J/mol
ν = kinematic viscosity, m^2/s
ρ = density, kg/m^3
σ_g = standard deviation of growth-rate distribution
σ_L = standard deviation of size distribution
Θ = transformed time, (mol/m^3)^g · s

Superscripts and subscripts

$-$ = mean value
$*$ = value at equilibrium
$\sim$ = total amount in the semibatch crystallizer
$'$ = variable in log-normal distribution
c = crystal
cr = critical size
f = fluid
ij = for the subpopulation, which was born in time step i and arrived to the semibatch reactor in time step j
r = reactant
s = solid
T_{mixer} = at the end of T-mixer
0 = initial

Literature Cited

Aoun, M., E. Plasari, R. David, and J. Villermaux, "A Simultaneous Determination of Nucleation and Growth Rates from Batch Spontaneous Precipitation," *Chem. Eng. Sci.*, **54**, 1161 (1999).

Armenante, P. M., and D. J. Kirwan, "Mass Transfer to Microparticles in Agitated Systems," *Chem. Eng. Sci.*, **44**, 2781 (1989).

Åslund, B., and Å. C. Rasmuson, "Semibatch Reaction Crystallization," *AIChE J.*, **38**, 328 (1992).

Bhandarkar, S., R. Brown, and J. Estrin, "Studies in Rapid Precipitation of Hydroxides of Calcium and Magnesium," *J. Cryst. Growth*, **97**, 406 (1989).

Bohlin, M., and Å. C. Rasmuson, "Modeling of Growth Rate Dispersion in Batch Cooling Crystallization," *AIChE J.*, **38**, 1853 (1992).

Bourgoin, M. E., "Memoire sur les Courbes de Solubilite des Acides Salicylique et Benzoique," *Ann. Chim. Phys.*, **15**, 161 (1878).

Calderbank, P. H., and M. B. Moo-Young, "The Continuous Heat and Mass-Transfer Properties of Dispersions," *Chem. Eng. Sci.*, **16**, 39 (1961).

Estrin, J., *Handbook of Industrial Crystallization*, Chap. 6, A. S. Myerson, ed., Butterworth-Heinemann, Boston (1992).

Fletcher, R., *Practical Methods of Optimization*, 2nd ed., Wiley, New York (1987).

Garside, J., and R. I. Ristic, "Growth Rate Dispersion Among ADP Crystals Formed by Primary Nucleation," *J. Cryst. Growth*, **61**, 215 (1983).

Gill, P. E., W. Murray, and M. H. Wright, *Practical Optimization*, Academic Press, London (1981).

Goeller, G. M., and A. Osol, "The Salting-Out of Molecular Benzoic Acid in Aqueous Salt Solutions at 35°C," *J. Amer. Chem. Soc.*, **59**, 2132 (1937).

Herz, W., and F. Hiebenthal, "Über Löslichkeitsbeeinflussungen," *Z. Anorg. Chem.*, **177**, 363 (1928).

Hoffmann, F., and K. Langbeck, "Studien über Löslichkeits-beeinflussung," *Z. Phys. Chem.*, **51**, 385 (1905).

Klug, D. L., and R. L. Pigford, "The Probability Distribution of Growth Rates of Anhydrous Sodium Sulphate Crystals," *Ind. Eng. Chem. Res.*, **28**, 1718 (1989).

Larsson, E., "Die Löslichkeit von Säuren und Salzlösungen: II. Die Löslichkeit der Benzoesäure und der Aktivitetskoeffizient ihrer Moleküle in wässerigen Benzoatlösungen," *Z. Phys. Chem.*, **148A**, 148 (1930a).

Larsson, E., "Die Löslichkeit von Säuren und Salzlösungen: III. Die Löslichkeit der Benzoesäure und der Aktivitetskoeffizient ihrer Moleküle in Lösung von Natriumchlorid und Kaliumchlorid," *Z. Phys. Chem.*, **148A**, 304 (1930b).

Levenspiel, O., *Chemical Reaction Engineering*, 2nd ed., Wiley International, New York (1972).

Mahajan, A. J., and D. J. Kirwan, "Rapid Precipitation of Biochemicals," *J. Phys. D: Appl. Phys.*, **26**, B176 (1993).

Mahajan, A. J., and D. J. Kirwan, "Nucleation and Growth Kinetics of Biochemicals Measured at High Supersaturations," *J. Cryst. Growth*, **144**, 281 (1994).

Mersmann, A., "Calculation of Interfacial Tension," *J. Cryst. Growth*, **102**, 841 (1990).

Mignon, D., T. Manth, and H. Offermann, "Kinetic Modelling of Batch Precipitation Reactions," *Chem. Eng. Sci.*, **51**, 2565 (1996).

Mohanty, R. S., Bhandarkar, B. Zuromski, R. Brown, and J. Estrin, "Characterizing the Product Crystals from a Mixing Tee Process," *AIChE J.*, **34**, 2063 (1988).

Mohanty, R., S. Bhandarkar, and J. Estrin, "Kinetics of Nucleation from Aqueous Solution," *AIChE J.*, **36**, 1536 (1990).

Nallet, V., D. Mangin, and J. P. Klein, "Model Identification of Batch Preciptations: Application to Salicylic Acid," *Comput. Chem. Eng.*, **22**, S649 (1998).

Nielsen, A. E., "Homogeneous Nucleation in Barium Sulphate Precipitation," *Acta Chem. Scand.*, **15**, 441 (1961).

Nielsen, A. E., *Kinetics of Precipitation*, Pergamon Press, Oxford (1964).

Nielsen, A. E., "Nucleation in Aqueous Solution," *Crystal Growth: Proc. ICCG-1*, H. S. Peiser, ed., Pergamon, Oxford, p. 419 (1967).

Nielsen, A. E., "Nucleation and Growth of Crystals at High Supersaturation," *Krist. Tech.*, **4**, 17 (1969).

Nielsen, A. E., "Electrolyte Crystal Growth Mechanism," *J. Cryst. Growth*, **67**, 289 (1984).

Nielsen, A. E., and O. Söhnel, "Interfacial Tensions Electrolyte Crystal-Aqueous Solution, from Nucleation Data," *J. Cryst. Growth*, **11**, 233 (1971).

Ostwald, W., "Über die Vermeintliche Isomeric des Roten und Gelben Quecksilberoxyds und die Oberfläschen Spannung Fester Körper," *Z. Phys. Chem.*, **34**, 495 (1900).

Ramanarayanan, K. A., M. A. Athreya, and M. A. Larson, "Statistical-Mathematical Modeling of CSD in Continuous and Batch Crystallizers," *AIChE Symp. Ser.*, **80**, 76 (1984).

Randolph, A. D., and E. T. White, "Modeling Size Dispersion in the Prediction of Crystal-Size Distribution," *Chem. Eng. Sci.*, **32**, 1067 (1977).

Randolph, A. D., and M. A. Larson, *Theory of Particulate Processes*, 2nd ed., Academic Press, San Diego (1988).

Rivera, T., and A. D. Randolph, "A Model for the Precipitation of Pentaerythritol Tetranitrate (PETN)," *Ind. Eng. Chem. Process Des. Dev.*, **17**, 182 (1978).

Schubert, H., and A. Mersmann, "Determination of Heterogeneous Nucleation Rates," *Trans. Inst. Chem. Eng.*, **74**, 821 (1996).

Seidell, A., *Solubility of Inorganic, Metallorganic and Organic Compounds*, 3rd ed., van Nostrand, New York (1940).

Söhnel, O., and J. W. Mullin, "A Method for the Determination of Precipitation Induction Periods," *J. Cryst. Growth*, **44**, 377 (1978).

Söhnel, O., and J. W. Mullin, "Interpretation of Crystallization Induction Periods," *J. Colloid Interfacial Sci.*, **123**, 43 (1988).

Söhnel, O., and J. Garside, *Precipitation*, Butterworth-Heinemann, Oxford (1992).

Tosun, G., "An Experimental Study of the Effect of Mixing on the Particle Size Distribution in $BaSO_4$ Precipitation Reaction," *Euro. Conf. on Mixing*, Pravia, Spain, p. 161 (1988).

Ward, H. L., and S. S. Cooper, "The System Benzoic Acid, Ortho Phthalic Acid, Water," *J. Phys. Chem.*, **34**, 1484 (1930).

Manuscript received Feb. 14, 2000, and revision received Nov. 2, 2000.